

Some aspects of the cosmogonic outward migration of Neptune

Co-planar migration

L. Neslušan and M. Jakubík

*Astronomical Institute of the Slovak Academy of Sciences
059 60 Tatranská Lomnica, The Slovak Republic, (E-mail: ne@ta3.sk;
mjakubik@ta3.sk)*

Received: July 3, 2013; Accepted: October 14, 2013

Abstract. Considering a simple model of the cosmogonic outward migration of Neptune, we investigate if the assumption of an extremely low orbital inclination of small bodies in a once-existing proto-planetary disk could influence the structure of reservoirs of the objects in the trans-Neptunian region. We found no significant influence. Our models predict only the existence of the mean-motion resonances (MMRs) with Neptune 2:3, 3:5, 1:2, and an anemic scattered disk (MMRs 3:4, 5:7, and 9:11 are also indicated). To explain the classical Edgeworth-Kuiper belt, relatively abundant 4:7 and 2:5 MMRs, and the more numerous scattered disk, we need to assume that, e.g., the outer boundary of the original proto-planetary disk considerably exceeded the distance of the current Neptune's orbit (Neptune probably ended its migration at the distance, where the disk's density started to be sub-critical), or that some Pluto-sized objects resided inside the MMRs and in the distant parts of the original proto-planetary disk.

Key words: TNOs – resonant component – Neptune migration

1. Introduction

The concept of planetary migration was suggested by Fernández and Ip (1984). Later, Malhotra (1993) demonstrated the sculpting the trans-Neptunian (TN, hereinafter) population by migrating Neptune. Many details in the TN structure have been, since then, explained with the help of the concept of Neptune's outward migration. Malhotra (1995) pointed out a significant fraction of TN objects being in the mean-motion resonances (MMRs, hereinafter) with Neptune and in orbits having the eccentricities in a wide range. Hahn and Malhotra (1999) simulated the common migration of Neptune and large planetesimals (10 to 200 Earth masses) and showed that the trapping of such large bodies to the resonances would not have occurred. Neptune had to migrate smoothly, interacting with much smaller objects. Gomes (2003) argued that the so-called "hot component" of the classical Kuiper belt has also its origin in the migration of Neptune. The formation of the TN population within the Neptune's outward

migration with the planetesimals locked in the MMRs with this planet was also demonstrated by Levison and Morbidelli (2003). Gomes et al. (2004) also investigated the phenomenon of planetary migration due to the scattering of disk planetesimals and found that Neptune had to migrate up to the end of the disk, which was situated near 30 AU (see also the review by Morbidelli and Brown, 2004).

It is now generally accepted that Saturn, Uranus, and Neptune were formed at shorter heliocentric distances than these planets reside at present (Fernández and Ip, 1984; Malhotra, 1993; Hahn and Malhotra, 1999; Morbidelli, 2004; Hahn and Malhotra, 2005; also according the Nice model: Tsiganis et al., 2005; Gomes et al. 2005). After an instability (e.g. Tsiganis et al., 2005; Gomes et al., 2005; Levison et al., 2008), Saturn increased its separation from Jupiter and ice giants, Uranus and Neptune, migrated outward especially due to their interaction with a disk of planetesimals, which was conserved beyond their initial formation site ranging from ~ 5.5 to ~ 14 AU from the Sun (Tsiganis et al., 2005; Gomes et al., 2005; Morbidelli et al., 2008). Only the small bodies trapped in the MMRs with Neptune occurred beyond its final orbit. This explains why there is by a factor of from 20 to 100 less matter than it would be in the case of the formation of the TN population in situ (Charnoz and Morbidelli, 2007). The scenario also explains the truncation of the classical TN belt at the MMR 1:2 with Neptune (Morbidelli et al., 2008), the outermost MMR to efficiently trap the small bodies.

In our work, we aim to contribute to a refinement of the Neptune's outward migration with respect to the structure of small bodies currently orbiting the Sun beyond Neptune. To reveal some potential relationships between the specific way of migration and the final TN structure, we consider several variations of a simple model of the migration process. Basically, we assume that the original planetesimal disk had the outer border at the current Neptune's orbit and the TN population occurred due to shifting outward some objects that were trapped into the resonance with Neptune and migrated with this planet.

Since the study is intended to be only our preliminary inspection of the problem, we consider only the single planet, Neptune, influencing massless test particles (TPs). This planet is forced to migrate using a simple, analytical model of the increase of its semi-major axis. The mass of the planet is assumed to be constant (Neptune acquired its current mass before the migration). The initial inclination of the Neptune's orbit is not known. In this paper, we focus on the simplest possibility that the inclination to the mean orbital plane of small bodies was zero.

Nor is the initial position of Neptune known. We thus assume three initial heliocentric distances of the planet in course to address the question, whether the initial position of Neptune, at the beginning of its migration, could be somehow important in creation of some specific features of the TN structure.

Due to a gaseous phase of the existence of the solar nebula, the solid particles obviously concentrated to the nebula's equatorial plane, therefore their orbits had extremely low inclinations to their mean orbital plane. These inclinations

could be comparable to those of the particles in the present Saturnian ring or, perhaps, even lower. The assumption of the extremely low inclinations is reasonable if the orbital planes of giant planets were highly aligned to each other. The long-period perturbations by these on the planetesimal disk could excite, in a certain degree, the eccentricities, since the component of gravitational force oriented in the common orbital plane of all bodies was present. However, the perpendicular component of the force could be absent, therefore the inclination could conserve itself to be original. Consequently, we are here especially interested in an impact of the assumption of low-inclination orbits onto the final structure of the TN population.

At the end, we compare the simulated and real radial distribution of the TN objects to decide if the concept of Neptune migration alone can be sufficient to explain the existence of all TN population, or some parts of it.

2. Simple model of migration

To create an easy-calculation, but a realistic model of the Neptune's outward migration, we adopt an assumption of the linear increase of the Neptune-orbit semi-major axis, during the considered first phase, and an assumption of an exponentially decreasing rate of the migration (semi-major axis) during the second considered phase.

The linear increase of the semi-major axis of the Neptune orbit, a_N , can be justified in the following consideration. The planet's mass m_N is considered to be constant. In fact, its increase in the process of planet's interaction with planetesimals during the migration was negligible. The increase of the impulse of the planet, $m_N \Delta v_N$ (Δv_N is the increase of the planet orbital velocity, v_N), within a time interval, Δt , is proportional to the total mass of encountered planetesimals, M_{ps} , within Δt and the net angular momentum of the encountered planetesimals, H_{ps} . The planetesimals are supposed to move around the Sun in almost circular (eccentricity, e , can be approximated by zero) and co-planar (inclination to the common orbital plane, i , can also be approximated by zero) orbits. In a close vicinity of Neptune, where the exchange of the angular momentum takes place, their mean semi-major axis, $\langle a \rangle$, is roughly equal to the actual semi-major axis of Neptune's orbit, i.e. $\langle a \rangle \approx a_N$.

Taking the above mentioned assumptions into account, the net angular momentum per unit mass of the planetesimals encountering Neptune can be given as

$$H_{ps} = \sqrt{\langle a \rangle (1 - e^2)} \cos i \approx \sqrt{a_N}. \quad (1)$$

The total mass of the planetesimals is proportional to their surface density, $\sigma_{ps} = \sigma_o r^{-3/2}$, and the length of the Neptune's trajectory per Δt , i.e. $v_N \Delta t$. Above, σ_o is a constant of proportionality and the heliocentric distance r can again be approximated by the Neptune's semi-major axis, i.e., $r \approx a_N$. So, the

change of the Neptune's momentum can be given as

$$m_N \Delta v_N \approx K_1 \sigma_o a_N^{-1} v_N \Delta t, \quad (2)$$

where K_1 is a constant of proportionality. From this relation, the Neptune's acceleration to migrate outward can be calculated as

$$\frac{\Delta v_N}{\Delta t} = \frac{K_1 \sigma_o}{m_N} a_N^{-1} v_N. \quad (3)$$

The Keplerian orbital velocity of Neptune can be expressed by a well-known relation

$$v_N = k \sqrt{M_\odot} \sqrt{\frac{2}{r} - \frac{1}{a_N}} \approx k \sqrt{M_\odot} a_N^{-1/2}, \quad (4)$$

where k is the Gauss gravitational constant, M_\odot is the mass of the Sun, and we again approximated $r \approx a_N$. Using this relation, the Neptune's acceleration is

$$\frac{\Delta v_N}{\Delta t} \approx -\frac{1}{2} k \sqrt{M_\odot} a_N^{-3/2} \frac{\Delta a_N}{\Delta t}. \quad (5)$$

Comparing (3) and (5), one can find that

$$\Delta a_N = K_a \Delta t, \quad (6)$$

where $K_a = -2K_1 \sigma_o / m_N$. After integration of this equation, we obtain simple, linear dependence of a_N on time, t . Specifically,

$$a_N = a_d + K_a t. \quad (7)$$

a_d is the semi-major axis of Neptune in time $t = 0$, i.e. at the beginning of the followed outward migration of this planet.

During the first phase Neptune scatters the planetesimals in its vicinity. The decrease of their number is compensated by the fact that the planet encounters new bodies at its shift outward. We assume a steady-state of the process of scattering and approaching new planetesimals. This steady-state ends when Neptune approaches the outer boundary of the planetesimal disk and the second phase of its migrations starts, in time $t = t_1$. Since it no longer passes any new bodies, the number of those encountered at the boundary must decrease, whereby we assume an exponential decrease of their number and, therefore, total mass. This mass is a function of time and can be given as

$$M_{ps} = M_1 \exp\left(-\frac{t - t_1}{\tau}\right). \quad (8)$$

M_1 is the mass of the planetesimal encountered within the time interval from t_1 to $t_1 + \Delta t$ and τ is a timescale characterizing the decay of the planetesimal disk at its outer border by Neptune.

Taking into account the mass given by relation (8), the change of Neptune's impulse is

$$m_N \Delta v_N \approx K_2 M_1 k M_\odot \exp[-(t - t_1)/\tau] \Delta t \quad (9)$$

in its second migration phase. K_2 is another constant of proportionality. Now, using relation (5), we can replace Δv_N with Δa_N and, after some obvious mathematical handling, to find the dependence of the Neptune's semi-major axis, a_N , on time in the second phase as

$$a_N = a_1 \left\{ 1 + K_b \left[1 - \exp\left(-\frac{t - t_1}{\tau}\right) \right] \right\}^{-2}, \quad (10)$$

where $K_b = K_2 M_1 \tau \sqrt{a_1} / m_N$ and a_1 is the semi-major axis of Neptune at the end of the first and beginning of the second phase of its migration.

It is reasonable to require the continuous behavior of the semi-major axis between both first and second phases of migration. This requirement implies that the time derivative of a_N in $t = t_1$ given by relation (7) must be equal to the time derivative of a_N in $t = t_1$ given by relation (10). Hence,

$$K_b = -\frac{K_a \tau}{2a_1}. \quad (11)$$

The fact that the first-phase migration starts at $a_N = a_d$ in time $t = t_o$ and ends at $a_N = a_1$ in time $t = t_1$ further implies (according to relation (7)) that

$$K_a = \frac{a_1 - a_d}{t_1 - t_o}. \quad (12)$$

Similarly, the second-phase migration starts at $a_N = a_1$ in time $t = t_1$ and ends at $a_N = a_2$ (the final semi-major axis a_2 can be identified to the semi-major axis of the current Neptune's orbit) in time $t = t_2$ yields

$$K_b = \left(\sqrt{\frac{a_1}{a_2}} - 1 \right) \left[1 - \exp\left(-\frac{t_2 - t_1}{\tau}\right) \right]^{-1}. \quad (13)$$

Supplying (11) into (13), we can K_b and derive a transcendent equation for τ in the form

$$\tau = \frac{2a_1}{K_a} \left(1 - \sqrt{\frac{a_1}{a_2}} \right) \left[1 - \exp\left(-\frac{t_2 - t_1}{\tau}\right) \right]^{-1}. \quad (14)$$

In our simulations, we use three models of the Neptune's migration differing from each other by the initial value of semi-major axis, a_d . Specifically, we consider a_d equal to 9, 12, and 17 AU. The lowest value is regarded as a minimum possible initial semi-major axis with respect to the considered orbit of Saturn. The largest value can, perhaps, be regarded as a maximum acceptable limit of the compact initial configuration of giant planets. Since Uranus and Neptune in

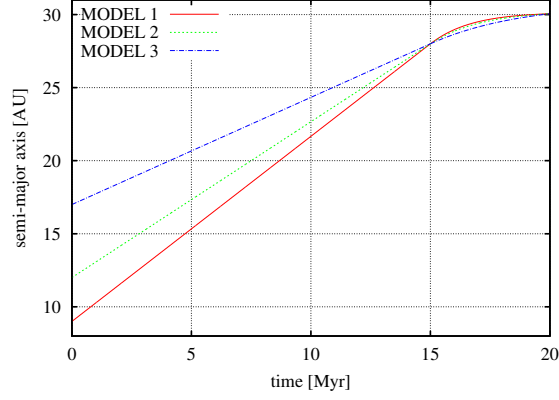


Figure 1. The evolution of the semi-major axis of the Neptune orbit during the outward migration of the planet according to the three models of the migration considered.

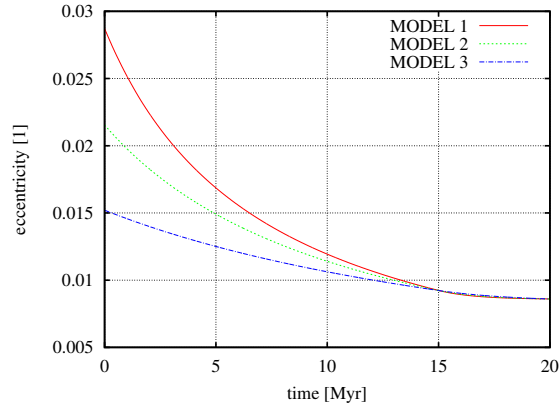


Figure 2. The evolution of the eccentricity of the Neptune orbit during the outward migration of the planet according to the three models of the migration considered.

this configuration used to be situated in a region between 10 and 15 AU, we also consider the medium value of semi-major axis. Further, we arbitrarily assume that the first phase lasts 15 Myr and ends at $a_1 = 28$ AU and the second phase lasts 5 Myr and ends when the planet occurs in its current orbit with the semi-major axis $a_2 = 30.058$ AU and eccentricity equal to 0.0086. The total period, 20 Myr, is regarded as a typical period of Neptune's outward migration. These combinations of parameters yield the values of τ equal to 1.613007, 1.990628, and 3.498434 Myr in the first, second, and third model considered, respectively. The eccentricity is damped during the migration. The final value of 0.0086 is

achieved by putting an appropriate initial value, which is found in an iteration. The evolutions of the semi-major axis and eccentricity of Neptune are illustrated in Figs. 1 and 2.

3. Model of a disk of small solid objects

Basically, we adopt the behavior of the surface density of solids, σ , depending on the heliocentric distance, r , according to Hayashi's model (1981) of the solid component of the proto-planetary disk, i.e. $\Sigma \propto r^{-3/2}$. In our simulations, the disk of planetesimals is represented by a set of 2000 massless TPs distributed by this law in the interval of heliocentric distance from r_{in} to r_{out} .

We assume the inner part of the disk already scattered due to the previous formation process of giant planets. The inner boundary of the considered disks, r_{in} , is set just 1 AU beyond the initial orbit of Neptune, depending on the model used. The outer border is set at the heliocentric distance of (i) $r_{out} = 30.5$ AU and (ii) $r_{out} = 60$ AU (Table 1). The first choice respects the fact that Neptune's outward migration ended at 30 AU, therefore the disk could not extend to a much larger distance. The second alternative is a toy model to see a wider context. After all, the initial planetesimal disk could still extend beyond the current orbit of Neptune, but its surface density was too low to enable a further planet migration due to the planet-planetesimal exchange of the orbital angular momentum.

Table 1. The initial characteristics of the performed simulations. The serial number of a given simulation is in the first column. Further notation: MNM - the model of Neptune migration (see Sect. 2), a_N - the initial semi-major axis of Neptune's orbit, r_{in} and r_{out} - the inner and outer boundaries of the considered disk of planetesimals, σ_e and σ_i - the values of the mean standard deviation characterizing the dispersion of eccentricity and inclination, respectively, of the initial TP orbits around their assumed zero values.

| sim. | MNM | a_N [AU] | r_{in} [AU] | r_{out} [AU] | σ_e | σ_i [rad] |
|------|-----|---------------|------------------|-------------------|------------|---------------------|
| 1 | 1 | 9 | 10 | 30.5 | 10^{-3} | 10^{-7} |
| 2 | 1 | 9 | 10 | 30.5 | 10^{-2} | 10^{-2} |
| 3 | 1 | 9 | 10 | 60.0 | 10^{-3} | 10^{-7} |
| 4 | 1 | 9 | 10 | 60.0 | 10^{-2} | 10^{-2} |
| 5 | 2 | 12 | 13 | 30.5 | 10^{-3} | 10^{-7} |
| 6 | 2 | 12 | 13 | 30.5 | 10^{-2} | 10^{-2} |
| 7 | 3 | 17 | 18 | 30.5 | 10^{-3} | 10^{-7} |
| 8 | 3 | 17 | 18 | 60.0 | 10^{-3} | 10^{-7} |

As mentioned in the Introduction, we aim to study the disk of solid objects extremely concentrated to the common orbital plane aligned with that of the Neptune orbit. Thus, we model the set of TPs with a randomly distributed inclination to the common plane, but with a characteristic dispersion having $\sigma_i = 10^{-7}$ rad (Table 1). The dispersion of eccentricity is assumed to be larger, with $\sigma_e = 10^{-3}$, since the formed giant planet acted on the small objects in the directions laying in the common plane (but a perpendicular component of their force can be regarded as negligible implying the extremely low inclination). As a reference, we also consider more dynamically excited disks with $\sigma_e = 10^{-2}$ and $\sigma_i = 10^{-2}$ rad.

4. Structure of the TN region formed

The first insight into the formed TN structure is the distribution of final TN orbits in the $a-e$ space shown in Fig. 3. Regardless the model considered, the TPs occurred in the TN region locked in, especially, three numerous MMRs with Neptune: 2:3, 3:5, and 1:2. A small number of the TPs are in 3:4 MMR. (In models 5–8, there is also a pattern of high, 9:11 MMR, and in models 7 and 8 MMR 5:7.) Some TPs are in the scattered disk. The latter is, however, much less abundant than the dominant MMRs 2:3, 3:5, and 1:2.

At the end of the simulations, no initial distribution is conserved in the models 1, 2, 5, 6, and 7 with the considered outer boundary at 30.5 AU. In models 3, 4, and 8, with the considered outer boundary at 60 AU, the initial distribution is completely destroyed up the first dominant MMR, 2:3, at about $a \sim 39$ AU. Then, it is destroyed in the region of the well-known strong instability in the interval $46.5 \lesssim a \lesssim 47.5$ AU. Otherwise, the initial distribution is largely conserved in these models.

The models with the considered initial outer boundary at 60 AU contain a significant number of TPs in the region of the classical Edgeworth-Kuiper belt situated in the interval of distances from about 42.5 to 45 AU. If the original disk spanned up to at least about the heliocentric distance of 45 AU, then the classical belt can be a more or less conserved outermost part of this disk. In models with the initial border at 30.5 AU, no pattern of the classical belt can be seen. Therefore, it seems improbable that this feature of the TN structure could form within the process of the small-body migration due to the trapping into the MMRs with Neptune.

The actual numbers of the TPs in the dominant MMRs 2:3, 3:5, and 1:2 in each considered model at the end of simulation are given in Table 2. As expected, MMR 2:3 is the most abundant of these three MMRs (except for model 8, where the number of TPs in MMR 1:2 slightly exceeds the number of TPs in MMR 2:3). This trends obviously occurs due to the close vicinity of the leading planet. However, the more distant MMR 1:2 is more abundant than the nearer 3:5 MMR in all models.

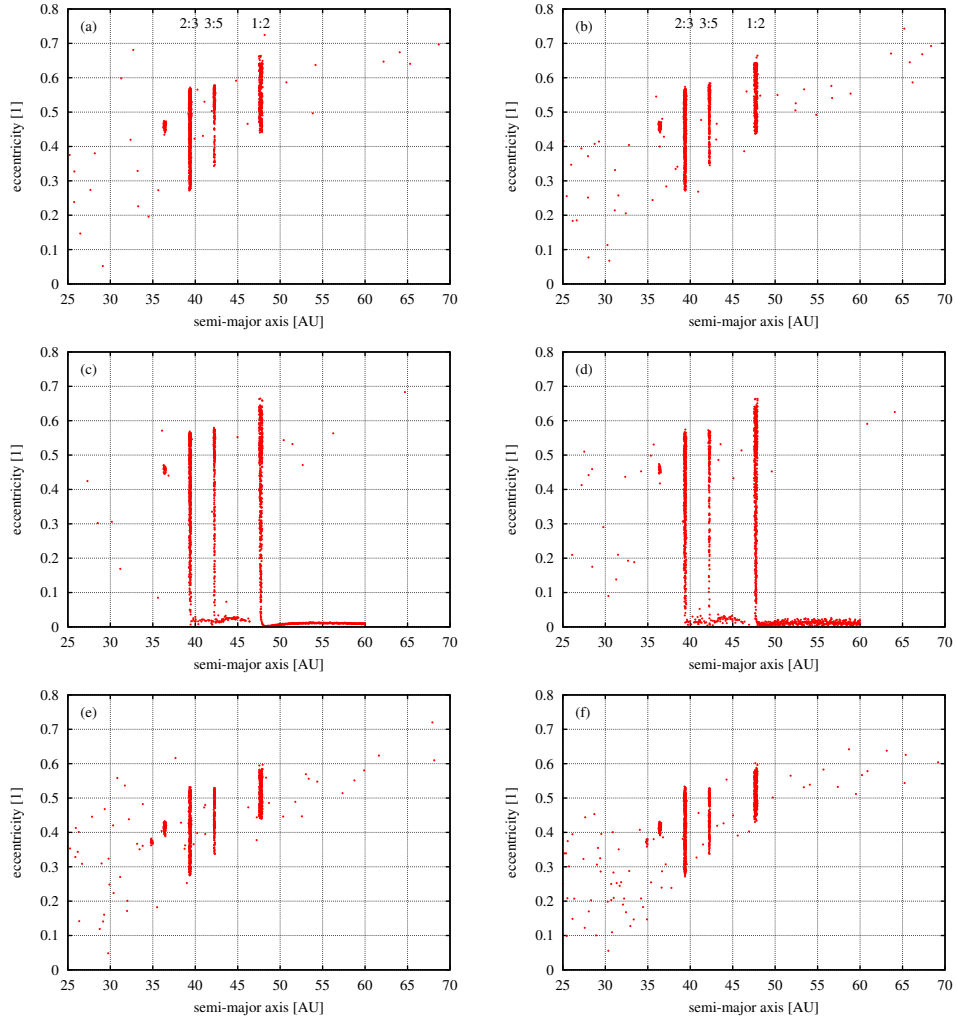


Figure 3. The distribution of the final orbits of theoretical TN particles at the end of migration in the eccentricity versus semi-major axis phase space (plots a–h for models 1–8, respectively, see Table 1). For model 8 (see plot h), the integration is performed up to 100 Myrs and the distribution in this time is shown in plot (i). The distribution of current orbits of real TN objects is shown in plot (j). (Plots g–j are shown on the next page.) The most abundant MMRs, 2:3, 3:5, and 1:2, are labeled in the top plots.

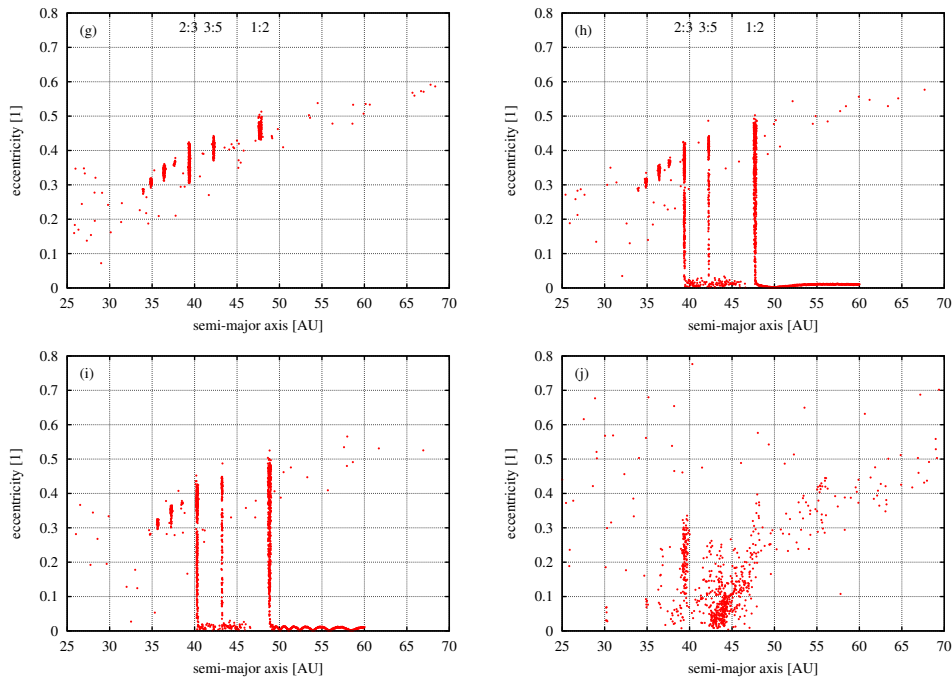


Figure 3. – continuation

If the outer boundary of the proto-planetary disk ended at 30.5 AU, as we assumed in models 1, 2, 5, 6, and 7, then the minimum eccentricity of the orbit of the objects in 2:3, 3:5, and 1:3 MMRs is relatively high, exceeding ~ 0.27 . If the outer boundary is at a larger heliocentric distance than the position of the outermost 1:2 MMR (our models 3, 4, and 8), the minimum eccentricity approaches zero. The maximum eccentricity of objects in the three MMRs does not seem to depend on the outer boundary and ranges from about 0.42 to 0.68 for all three MMRs and all considered models.

A short time after the migration ended, a prevailing majority of orbital inclinations still remain close to the initial values. Only a small number of TPs can be found, obviously after former close encounters with Neptune, in relatively high-inclination orbits. This i -excitation is typically up to $i \sim 30^\circ$ (in models 7 and 8 up to 20°). In fact, the currently observed higher inclinations, typically up to $\sim 40^\circ$, could be caused by other mechanism(s) than the gravitational perturbation of Neptune, e.g. by perturbations of some more massive bodies, like Pluto, inside the migrating TN population itself. (Or, the orbit of Neptune was not aligned, due to perturbations by the other giant planets on this orbit, to the mean orbital plane of small bodies. This scenario will be studied in a future work.)

The numbers of TPs in 2:3 MMR (Table 2) at the end of migration depends on the radial speed of the migration, which is greater in models 1–4 than in models 5 and 6, and the latter is greater than that in models 7 and 8. The same, or a slightly larger number of TPs are captured into 2:3 MMR in the models with the extreme low initial inclination, $i = 10^{-7}$ rad, (models 1, 3, 5) than the corresponding models with initial $i = 10^{-2}$ rad (models 2, 4, and 6, respectively).

The variation of the number of the TPs trapped in 3:5 MMR is, more or less, chaotic. In 1:2 MMR, significantly more TPs are trapped in the models with the outer boundary at 60 AU (models 3, 4, and 8) than in those with the boundary in 30.5 AU. Obviously, a lot of TPs initially situated in the region beyond 30.5 AU are trapped in this MMR.

Table 2. The non-corrected numbers of TPs in the MMRs 2:3, 3:5, and 1:2 as obtained in the considered models (characterized in Table 1).

| model: | 1 | 2 | 3 | 4 | 5 | 6 | 7 | 8 |
|--------|--------------------------------------|-------|-------|-------|-------|-------|-------|-------|
| MMR | | | | | | | | |
| | absolute numbers | | | | | | | |
| 2:3 | 859 | 823 | 715 | 712 | 591 | 604 | 469 | 467 |
| 3:5 | 211 | 265 | 245 | 204 | 207 | 194 | 146 | 178 |
| 1:2 | 368 | 346 | 517 | 555 | 378 | 372 | 310 | 479 |
| | relative numbers to those in MMR 2:3 | | | | | | | |
| 3:5 | 0.246 | 0.322 | 0.343 | 0.287 | 0.350 | 0.321 | 0.311 | 0.381 |
| 1:2 | 0.428 | 0.420 | 0.723 | 0.779 | 0.640 | 0.616 | 0.661 | 1.026 |

The actual numbers of the theoretical particles cannot be directly compared to the corresponding numbers of real TN objects because of the observational bias. We know that a discovery of any object depends on its apparent brightness. In more detail, the discovery probability is proportional to the time during which the object has its apparent brightness above a threshold and is situated in the night sky. Of course, there are other factors, as the object's albedo or behavior of its light curve, influencing the discovery probability.

To make a comparison with observations, we estimate the relative discovery probabilities of the objects in the considered MMRs and correct the obtained actual numbers with respect to these probabilities. It would be difficult, if not impossible, to take into account all the factors influencing the probability. So, we adopt some assumptions leading to a simplification of the probability determination. First, we assume that the directional distribution of all TN objects is homogeneous, i.e. the same number of objects are situated in the opposition to any position of the Earth in its orbit. Second, let all objects have the same albedo, A , and their differential size distribution can be described by the power law $n(R) = N_o R^{-s}$, where N_o is a gauging constant and s is the index of slope.

Table 3. The relative numbers of TPs in the MMRs 2:3, 3:5, and 1:2 corrected with respect to the main observational selection effects (see Sect. 4) as obtained in the considered models (characterized in Table 1). In three sections of the table, the numbers are listed for three values of the index of TN-population-size distribution, s . In the first part of each section, the numbers are given relatively to the number of TPs in 2:3 MMR in model 1 for $s = 4.0$. In the second part, the ratio of the corrected number of 3:5 MMR (1:2 MMR) and 2:3 MMR in the given model is presented.

| model: MMR | 1 | 2 | 3 | 4 | 5 | 6 | 7 | 8 |
|---------------|-------|-------|-------|-------|-------|-------|-------|-------|
| for $s = 3.8$ | | | | | | | | |
| 2:3 | 0.447 | 0.436 | 0.293 | 0.282 | 0.223 | 0.231 | 0.116 | 0.092 |
| 3:5 | 0.139 | 0.157 | 0.094 | 0.084 | 0.075 | 0.068 | 0.033 | 0.029 |
| 1:2 | 0.211 | 0.190 | 0.167 | 0.174 | 0.125 | 0.123 | 0.055 | 0.043 |
| ----- | | | | | | | | |
| 3:5 | 0.311 | 0.360 | 0.322 | 0.299 | 0.335 | 0.295 | 0.286 | 0.314 |
| 1:2 | 0.471 | 0.435 | 0.572 | 0.615 | 0.561 | 0.534 | 0.478 | 0.470 |
| for $s = 4.0$ | | | | | | | | |
| 2:3 | 1.000 | 0.976 | 0.645 | 0.619 | 0.483 | 0.499 | 0.237 | 0.185 |
| 3:5 | 0.316 | 0.354 | 0.209 | 0.187 | 0.161 | 0.146 | 0.067 | 0.058 |
| 1:2 | 0.481 | 0.429 | 0.374 | 0.386 | 0.269 | 0.265 | 0.112 | 0.083 |
| ----- | | | | | | | | |
| 3:5 | 0.316 | 0.363 | 0.323 | 0.302 | 0.333 | 0.292 | 0.285 | 0.313 |
| 1:2 | 0.481 | 0.440 | 0.579 | 0.624 | 0.557 | 0.530 | 0.471 | 0.449 |
| for $s = 4.2$ | | | | | | | | |
| 2:3 | 2.250 | 2.198 | 1.431 | 1.368 | 1.051 | 1.087 | 0.487 | 0.375 |
| 3:5 | 0.720 | 0.802 | 0.464 | 0.416 | 0.347 | 0.314 | 0.138 | 0.117 |
| 1:2 | 1.103 | 0.979 | 0.841 | 0.867 | 0.580 | 0.571 | 0.226 | 0.161 |
| ----- | | | | | | | | |
| 3:5 | 0.320 | 0.365 | 0.324 | 0.304 | 0.330 | 0.289 | 0.284 | 0.311 |
| 1:2 | 0.490 | 0.445 | 0.588 | 0.633 | 0.552 | 0.526 | 0.464 | 0.430 |

The apparent brightness, m , can be calculated from a well-known relation

$$m = m_{\odot} - 2.5 \log_{10}[A\Phi(\alpha)R^2] + 5 \log_{10}(1.496 \times 10^8 r r_g), \quad (15)$$

where m_{\odot} is the apparent magnitude of the Sun, $\Phi(\alpha)$ is the *Bowell et al.*'s (1989) phase function depending on the phase angle α , and r and r_g are the heliocentric and geocentric distances of the object in astronomical units (mean radius of the object, R , has to be then given in kilometers). In accordance with the discussion in the paper by *Neslušan and Paulech* (2006), we assume that the objects are discovered mainly around the opposition, where $r_g \approx r - 1$ and $\alpha \sim 0$, yielding $\Phi \sim 1$. We also adopt the red magnitude of the Sun (red magnitude is more relevant for the reflectance of TNO surfaces than the visual one) equal to -27.1 and albedo $A \approx 0.04$.

The given object moves from a distance r to $r + \Delta r$ (as well as vice versa) during a time interval Δt . This interval can be found by solving the appropriate Kepler problem.

Let every single TP represents a swarm of objects of all sizes distributed according to the assumed power-law distribution. Of these objects, there can be discovered only those with the apparent brightness higher than a certain limiting brightness characterized by the magnitude m_{lim} . Since the apparent brightness is proportional to the size of the object, i.e. its radius R , all objects with R larger than a critical radius R_{lim} can be discovered. With respect to relation (15), the critical radius for a chosen value of limiting magnitude m_{lim} can be calculated as

$$R_{lim} \approx \frac{1.496 \times 10^8}{\sqrt{A} 10^{0.2(m_{lim} - m_{\odot})}} r(r - 1). \quad (16)$$

Therefore, the contribution of a given TP to the discovery probability during its motion from r to $r + \Delta r$ and $r + \Delta r$ down to r is $\Delta p = 2\Delta t N_o R^{-s}$. Since we aim to determine the relative probability, the constant N_o can be chosen arbitrarily.

To obtain the total contribution of the TP to the probability, we sum all contributions from the particle's perihelion to such a distance, where R_{lim} reaches the maximum size of TN objects (~ 1200 km). The total relative number of the TPs in a given MMR is then the sum of the total probability contributions of all TPs in that MMR.

The corrected relative numbers of TPs in MMRs 2:3, 3:5, and 1:2 in our models are given in Table 3. Since the index of slope, s , of the resonant TN objects is not known, we consider three values of this free parameter. To compare these numbers with their observed counterparts, we consider the TN resonant objects detected in the CFEPS (Canada-France Ecliptic Plane Survey; Gladman et al., 2012). Although the numbers of the objects in the MMRs within this survey are smaller than the total numbers of known objects in the MMRs, we prefer to use the much more homogeneous data from the survey than a sample compiled often from the random discoveries by different instruments. The randomly collected data may bias the relative numbers of the objects in the individual MMRs. We use the database of all cataloged minor bodies (downloaded from the IAU Minor Planet Center, <http://www.minorplanetcenter.net/iau/MPCORB.html>, on April 11, 2013), from which we selected only the objects observed in three and more oppositions to construct the situation of these bodies in the $a-e$ phase space shown in Fig. 3j.

The absolute as well as relative-to-2:3-MMR numbers of objects in the most abundant actual MMRs with Neptune detected within the CFEPS are given in Table 4. One or two objects were found also in another, low abundant MMRs, not listed in the table. The first partial conclusion drawn from the comparison of the relative numbers in our models and in reality is that MMRs 4:7 and 2:5 as well as the classical Edgeworth-Kuiper belt are probably not the result of the trapping the bodies into MMRs and their common migration with Neptune.

Table 4. The numbers of the TN objects in the main MMRs with Neptune detected within the CFEPS (Gladman et al., 2012). Specifically, we take the absolute numbers of detected objects, N_{abs} , and also calculate the ratio of the number of the objects in the given MMR and number in the most abundant MMR 2:3, i.e the relative number, N_{rel} .

| MMR | 2:3 | 3:5 | 1:2 | 4:7 | 2:5 | 3:4 |
|-----------|-------|-------|-------|-------|-------|-------|
| N_{abs} | 24 | 6 | 5 | 5 | 5 | 4 |
| N_{rel} | 1.000 | 0.250 | 0.208 | 0.208 | 0.208 | 0.167 |

Our result concerning the absence of 4:7 and 2:5 MMRs is consistent with an earlier study by Chiang et al. (2003). Since the semi-major axes of objects in MMR 4:7 (~ 43.6 AU) are within the interval of orbits in the densest core of the classical belt (from about 42.5 to 45 AU - see Fig. 4j), both these TN structures have, likely, the common origin, different from the migration process.

According to all our models, MMRs 3:5 and, especially, 1:2 should be significantly more abundant relatively to the abundance of 2:3 MMR. The reason for the underestimate of these two MMRs is still unknown. We can only state that the considered size distribution (assumed value of index s) is, obviously, of no importance. Though the absolute numbers of the TPs trapped in the migrating MMRs largely vary with the varying s , the relative numbers remain essentially the same.

In models with the outer boundary at 60 AU (3, 4, and 8), a significant part of the initial population is conserved beyond all three dominant MMRs. The conserved part beyond 2:3 and 3:5 MMRs could be excited, in a further evolutionary period, and become the classical Edgeworth-Kuiper belt, from which the abundant 4:7 MMR (Table 4) could form. To see whatever an excitation trend occurs, we integrated the orbits of TPs in model 8 for another 80 Myrs. The distribution of the TPs in the e - a space is shown in Fig. 3i. Comparing this plot for 100 Myr evolution to the corresponding Fig. 3h for 20 Myr evolution, we cannot observe any significant excitation of eccentricity. Nor can a significant excitation of inclination be found. Probably, other mechanism had to be efficient to excite the orbits (e.g., perturbations by some Pluto-sized objects inside this region), if the classical belt is actually evolved from the remnant of the initial population beyond 2:3 and 3:5 MMRs.

A slow process of escape from the MMRs, which were filled in within the process of migration, could likely be a source of objects replenishing the scattered disk. Its abundance is predicted too low by the scenario of the migration alone.

5. Conclusion

The simple model of Neptune outward migration can explain the transport of the objects in the present TN region, regardless of the fact whether the initial orbital inclinations of these objects are extremely low or moderately low.

However, the full consistency with the current, observed TN structure is not achieved. We need to invoke another mechanisms to explain especially the existence of the classical Edgeworth-Kuiper belt, relative abundant MMRs with Neptune 4:7 and 2:5, as well as the richer scattered disk.

Maybe, there were (still are) some larger, Pluto-sized objects in the appropriate regions. These objects have scattered smaller bodies out of the MMRs formed during the migration and the latter then have moved to the classical belt, scattered disk, or other MMRs. It is not even excluded that the original proto-planetary disk extended far beyond the current orbit of Neptune and the classical belt and other, non-predicted MMRs, formed from this initial population. Then, it will be necessary to prove that Neptune could migrate only inside the part of the proto-planetary disk with an overcritical density, whereby the density decreased below critical just at its current orbit. We believe that future studies will clarify the above mentioned questions.

Acknowledgements. This work has been supported, in part, by the VEGA - the Slovak Grant Agency for Science (grant No. 0011).

References

- Bowell, E., Hapke, B., Domingue, D., Lumme, K., Peltoniemi, J., Harris, A.: 1989, in *Asteroids II*, eds.: R. Binzel, T. Gehrels, and M. Matthews, Univ. Arizona Press, Tucson, 524
- Charnoz, S., Morbidelli, A.: 2007, *Icarus* **188**, 468
- Chiang, E.I., Lovering, J.R., Millis, R.L., Buie, M.W., Wasserman, L.H., Meech, K.J.: 2003, *Earth, Moon, Planets* **92**, 49
- Fernández, J.A., Ip, W.H.: 1984, *Icarus* **58**, 109
- Gladman, B., Lawler, S.M., Petit, J.-M., Kavelaars, J., Jones, R.L., Parker, J.Wm., Van Laerhoven, C., Nicholson, P., Rousset, P., Bieryla, A., Ashby, M.L.N.: 2012, *Astron. J.* **144**, id.23
- Gomes, R.S.: 2003, *Icarus* **161**, 404
- Gomes, R.S., Morbidelli, A., Levison, H.F.: 2004, *Icarus* **170**, 492
- Gomes, R., Levison, H.F., Tsiganis, K., Morbidelli, A.: 2005, *Nature* **435**, 466
- Hahn, J.M., Malhotra, R.: 1999, *Astron. J.* **117**, 3041
- Hahn, J.M., Malhotra, R.: 2005, *Astron. J.* **130**, 2392
- Hayashi, C.: 1981, *Prog. Theor. Phys. Suppl.* **70**, 35
- Levison, H.F., Morbidelli, A.: 2003, *Nature* **426**, 419
- Levison, H.F., Morbidelli, A., VanLaerhoven, C., Gomes, R., Tsiganis, K.: 2008, *Icarus* **196**, 258
- Malhotra, R.: 1993, *Nature* **365**, 819
- Malhotra, R.: 1995, *Astron. J.* **110**, 420

- Morbidelli, A.: 2004, *Science* **306**, 1302
- Morbidelli, A., Brown, M.E.: 2004, in *Comets II*, eds.: M. C. Festou, H. U. Keller, and H. A. Weaver, Univ. Arizona Press, Tucson, 175
- Morbidelli, A., Levison, H.F., Gomes, R.: 2008, in *Solar System beyond Neptune*, eds.: M. A. Barucci, H. Boehnhardt, D. P. Cruikshank, and A. Morbidelli, Univ. Arizona Press, Tucson, 275
- Neslušan, L., Paulech, T.: 2006, *Contrib. Astron. Obs. Skalnaté Pleso* **36**, 158
- Tsiganis, K., Gomes, R., Morbidelli, A., Levison, H.F.: 2005, *Nature* **435**, 459